JOURNAL OF AIRCRAFT
Vol. 47, No. 4, July–August 2010

Transonic Aeroelastic Stability Predictions Under the Influence of Structural Variability

S. Marques,* K. J. Badcock,† H. H. Khodaparast,‡ and J. E. Mottershead§
University of Liverpool, L69 3BX, United Kingdom

DOI: 10.2514/1.46971

Flutter prediction as currently practiced is almost always deterministic in nature, based on a single structural model that is assumed to represent a fleet of aircraft. However, it is also recognized that there can be significant structural variability, even for different flights of the same aircraft. The safety factor used for flutter clearance is in part meant to account for this variability. Simulation tools can, however, represent the consequences of structural variability in the flutter predictions, providing extra information that could be useful in planning physical tests and assessing risk. The main problem arising for this type of calculation when using high-fidelity tools based on computational fluid dynamics is the computational cost. The current paper uses an eigenvalue-based stability method together with Euler-level aerodynamics and different methods for propagating structural variability to stability predictions. The propagation methods are Monte Carlo, perturbation, and interval analysis. The feasibility of this type of analysis is demonstrated. Results are presented for the Goland wing and a generic fighter configuration.

Nomenclature

Latin Symbols

A	=	Jacobian matrix
b	=	optimization problem constraints
$\mathcal{C}$	=	cost function for interval optimization problem
E	=	Young's modulus of elasticity
G	=	shear modulus
$\mathbf{g}$	=	the first Jacobian of γ_i with respect to θ
H	=	optimization objective function Hessian
$\mathcal{L}$	=	Lagrangian function
p	=	eigenvector
$\mathbf{R}$	=	residual vector of the fluid and/or structural model
S	=	Schur-complement matrix
t	=	thickness
$\mathbf{w}$	=	vector of fluid and/or structural unknowns
Var	=	Variance

Greek Symbols

γ_i	=	either the real or imaginary part of an aeroelastic eigenvalue
λ	=	eigenvalue
μ	=	bifurcation parameter (altitude)
φ	=	Lagrangian multiplier vector
θ	=	m-dimensional vector containing the m uncertain structural parameters

Subscripts or superscripts

f	=	fluid model
s	=	structural model
0	=	equilibrium
$\hat{\theta}$	=	the mean value of θ

Presented as Paper 2009-2324 at the 50th AIAA/ASME/ASCE/AHS/ASC Structures, Structural Dynamics, and Materials Conference 17th AIAA/ASME/AHS Adaptive Structures Conference 11th AIAA No, Palm Springs California, 4–7 May 2009; received 1 September 2009; accepted for publication 15 November 2009.

*Research Assistant, Department of Engineering. Member AIAA.
†Professor, Department of Engineering. Senior Member AIAA. Corresponding author.
‡Research Assistant, Department of Engineering.
§Professor, Department of Engineering.

I. Introduction

AN IMPORTANT area for research is how to account for variability in aeroelastic [1] and aerodynamic analysis [2]. Uncertainty can be classified into two categories. Aleatory uncertainty includes randomness in parameters. Epistemic uncertainty includes limitations in knowledge or lack of understanding and uncertainty due to human error. Several methodologies have been developed to introduce the effects of uncertainty into design procedures or engineering analysis. Two popular classes of methods have emerged [2]: probabilistic methods include Monte Carlo, moment methods, and polynomial chaos; nonprobabilistic methods include interval analysis and error propagation with sensitivity derivatives. The contribution of this paper is to consider how uncertainty in structural parameters can be efficiently propagated to aeroelastic stability predictions when expensive computational fluid dynamics (CFD)-level aerodynamics is used.

Structural variability arises from several sources, such as manufacturing tolerances, material differences, and wear. A study of the McDonnell Douglas F-4 Phantom II [3] quantified the weight and inertia variability for this aircraft, showing changes in mass and inertias of control surfaces by up to 15%. Quantifying uncertainty has been a subject of interest in the structures community for several years and numerous methods have been used [4,5].

In this work, the critical structural parameters for influencing aeroelastic stability are first identified, and then an estimate of the possible distribution or range of these parameters is made. This variability can then be propagated to a distribution in the flutter speed through an analysis code. This approach was previously taken for the Goland wing [6], with linear analysis used to compute the flutter speed. This is computationally efficient since the aerodynamic matrices can be precomputed and then used for all normal mode sets arising from the varying structural parameters. The probability density functions for the flutter speeds were computed, and some critical cases identified which were then recomputed using a time domain transonic small disturbance code. Willcox and Peraire [7] applied a two-dimensional time domain Euler CFD code to assess the impact of variability in structural frequencies of bladed disks and the effects in the tuning of cascades. Blade structural variability was

translated into a frequency probability density function (PDF) and the coupled aeroelastic system was solved making use of reduced order model (ROM) methods. Verhoosel et al. [8] used a monolithic fluid-structure interaction (FSI) code to model panel flutter with variability in the Young's modulus. In this case, the fluid flow was described by a two-dimensional unsteady linearized potential equation, and the structure was modeled by the Euler–Bernoulli beam equation. The parameter variability was represented by a Gaussian distribution obtained from a Karhunen–Loeve expansion and used perturbation methods. Rao and Majumder [9] applied interval analysis to a structural optimization problem under atmospheric uncertainty. Interval analysis finds the upper and lower extremes for possible response to parametric variation. The parameters were allowed to deviate $\pm 0.5\%$ from the nominal values. The structure was optimized for a gust response with constraints on flutter Mach number, weight, and energy. The authors concluded that interval analysis provides comparable results to probabilistic methods and should be used where probability distributions are difficult to obtain. Propagation methods were considered in reference [10] where interval, Monte Carlo, response-surface, and perturbation methods are compared for propagating structural variability through linear flutter calculations.

An extra difficulty is introduced when CFD-level aerodynamics is used for the aeroelastic analysis, namely the computational cost. Methods have been under development to reduce the cost of computing transonic flutter speeds using CFD methods for the aerodynamics [11]. These methods provide a suitable framework for doing analysis for the effects of stuctural variability since they operate on the aeroelastic modes. The modes of interest can be identified and analyzed for dependence on the uncertain structural parameters. There are several ways in which this can be done including the Monte Carlo method, perturbation methods, and interval analysis.

The purpose of this paper is to investigate the practicality of using CFD-derived aerodynamics when calculating the influence of structural variability on aeroelastic stability. The stability and variability propagation methods are described and then results are presented for the Monte Carlo and perturbation methods, and interval analysis applied to the Goland wing and a generic fighter. The emphasis is placed on demonstrating that eigenvalue-based stability calculations (with Euler-level aerodynamics) are computationally efficient enough to allow the variability analysis.

II. Aeroelastic Stability Formulation

The semidiscrete form of the coupled CFD–finite-element-method (FEM) system is written as

$$\frac{\mathrm{d}\mathbf{w}}{\mathrm{d}t} = \mathbf{R}(\mathbf{w}, \mu) \tag{1}$$

where

$$\mathbf{w} = [\mathbf{w}_f, \mathbf{w}_s]^T \tag{2}$$

is a vector containing the fluid unknowns $\mathbf{w}_f$ and the structural unknowns $\mathbf{w}_s$, and

$$\mathbf{R} = [\mathbf{R}_f, \mathbf{R}_s]^T \tag{3}$$

is a vector containing the fluid residual $\mathbf{R}_f$ and the structural residual $\mathbf{R}_s$. The residual also depends on a parameter μ (in this paper μ is altitude), which is independent of $\mathbf{w}$. An equilibrium $\mathbf{w}_0$ of this system satisfies $\mathbf{R}(\mathbf{w}_0, \mu) = \mathbf{0}$.

The flow solver used for this study is based on the University of Liverpool parallel multiblock solver. The Euler equations are discretized on curvilinear multiblock body-conforming grids using a cell-centered finite-volume method. The residual is formed using Osher's approximate Riemann solver [12] with monotone upwind scheme for conservation laws interpolation [13]. More details on the flow solver can be found in Badcock et al. [14].

The linear stability of equilibria of Eq. (1) is determined by eigenvalues of the Jacobian matrix $A = \partial\mathbf{R}/\partial\mathbf{w}$. In the current work a stability analysis is done based on the coupled-system Jacobian matrix which includes the Jacobian of the CFD residual with respect to the CFD and structural unknowns. The calculation of the Jacobian A is most conveniently done by partitioning the matrix as

$$A = \begin{bmatrix} \frac{\partial \mathbf{R}_f}{\partial \mathbf{w}_f} & \frac{\partial \mathbf{R}_f}{\partial \mathbf{w}_s} \\ \frac{\partial \mathbf{R}_s}{\partial \mathbf{w}_f} & \frac{\partial \mathbf{R}_s}{\partial \mathbf{w}_s} \end{bmatrix} = \begin{bmatrix} A_{ff} & A_{fs} \\ A_{sf} & A_{ss} \end{bmatrix} \tag{4}$$

The details of the Jacobian calculation are given in [15,16].

In the current work, and as is conventional in aircraft aeroelasticity, the structure is modeled by a small number of modes, and so the number of the fluid unknowns is far higher than the structural unknowns. This means that the Jacobian matrix has a large, but sparse, block A_{ff} surrounded by thin strips for A_{fs} and A_{sf}. As described in [11] the stability calculation is formulated as an eigenvalue problem, focusing on eigenvalues of the coupled system that originate from the uncoupled block A_{ss}.

Write the coupled system eigenvalue problem as

$$\begin{bmatrix} A_{ff} & A_{fs} \\ A_{sf} & A_{ss} \end{bmatrix} \mathbf{p} = \lambda \mathbf{p} \tag{5}$$

where $\mathbf{p} = [\mathbf{p}_f, \mathbf{p}_s]^T$ and λ are the complex eigenvector and eigenvalue, respectively. The eigenvalue λ (assuming it is not an eigenvalue of A_{ff}) satisfies [17] the nonlinear eigenvalue problem

$$S(\lambda)\mathbf{p}_s = \lambda \mathbf{p}_s \tag{6}$$

where $S(\lambda) = A_{ss} - A_{sf}(A_{ff} - \lambda I)^{-1} A_{fs}$.

Equation (6) is solved using Newton's method. Each iteration requires the formation of the residual $S(\lambda)\mathbf{p}_s - \lambda\mathbf{p}_s$ and its Jacobian matrix. The calculation of the correction matrix $A_{sf}(A_{ff} - \lambda I)^{-1}A_{fs}$ is required to form the Jacobian matrix with respect to $\mathbf{p}_s$ and λ. This can be achieved through $2n$ solutions of a linear system against $A_{ff} - \lambda I$, one for each column of A_{fs} with n being the number of normal modes retained. These solutions are then multiplied against A_{sf}. Now, for each value of the bifurcation parameter, there are multiple solutions of the nonlinear system in Eq. (6), and so the cost of forming the correction matrix at each Newton step, for each solution, and for a range of structural parameters becomes too high. To overcome this the expansion

$$(A_{ff} - \lambda I)^{-1} = A_{ff}^{-1} + \lambda A_{ff}^{-2} + \lambda^2 A_{ff}^{-3} + \ldots \tag{7}$$

is used where λ must be small for the series to converge. Note that this assumption is not restrictive since we assume that the eigenvalue we are calculating is a small change from the eigenvalue λ_0 of A_{ss}. Then λ_0 can be used as a shift to the full-system eigenvalue problem by replacing A_{ff} by $A_{ff} - \lambda_0 I$ and A_{ss} by $A_{ss} - \lambda_0 I$. This modifies the nonlinear eigenvalue problem in Eq. (6) by redefining $S(\lambda) = (A_{ss} - \lambda_0 I - \lambda I) - A_{sf}(A_{ff} - \lambda_0 I - \lambda I)^{-1} A_{fs}$. The series approximation then becomes

$$\begin{aligned}(A_{ff} - \lambda_0 I - \lambda I)^{-1} = {} & (A_{ff} - \lambda_0 I)^{-1} + \lambda (A_{ff} - \lambda_0 I)^{-2} \\ & + \lambda^2 (A_{ff} - \lambda_0 I)^{-3} + \ldots\end{aligned} \tag{8}$$

When the shifted problem is solved for λ, the eigenvalue of the original system is then $\lambda_0 + \lambda$. The terms $(A_{ff} - \lambda_0 I)^{-1} A_{fs}$ and $(A_{ff} - \lambda_0 I)^{-2} A_{fs}$ can be precomputed to yield the series approximation, which can then be evaluated for any λ at virtually no computational cost.

This method is referred to as the Schur method. Two forms are available. In both cases the series approximation is used for approximating the Jacobian matrix of the residual from Eq. (6). For the residual the evaluation of $S(\lambda)\mathbf{p}_s - \lambda\mathbf{p}_s$ can be made based on an exact evaluation (referred to as *full* in this paper) which requires the solution of one linear system against the right-hand side $A_{fs}\mathbf{p}_s$ or can

use the series approximation (referred to as *series*) at virtually no additional cost after the series matrices are formed.

III. Variability Formulation

A. Eigenvalue Calculations

In this paper we assume that the values of some structural model parameters θ are uncertain, defined either through a probability density function or by an interval of equally possible values. In either case we can define a mean or midpoint value. The building block for the propagation of the uncertainty in the structural parameters to the uncertainty in the aeroelastic eigenvalues is the ability to evaluate the eigenvalue at low cost for any desired value of the parameter vector θ. This is done in the following way. The matrices for the series approximation in Eq. (7) are first evaluated at the mean or midpoint value, denoted $\hat{\theta}$. This series approximation is then used to drive the Newton convergence to the aeroelastic eigenvalues for any normal mode set derived from the required value of $\hat{\theta}$. The residual $S(\lambda)\mathbf{p}_s - \lambda\mathbf{p}_s$ must be evaluated using the full evaluation since the series approximation is only valid for the mean or midpoint structural parameters. In this way the aeroelastic eigenvalue for a modified normal mode set can be obtained in a small number of additional linear solves once the mean parameter series approximation to S is calculated. This approach is at the heart of the propagation methods now described.

B. Monte Carlo Simulation

In a Monte Carlo process a large number of samples of the uncertain structural parameters θ is generated according to the assumed parameter probability density function. In the current work this leads to different normal mode shapes and frequencies, which are then used for the aeroelastic calculations. The respective response values γ_i (either the real or imaginary part of the ith eigenvalue) are evaluated using the Schur method as described in the previous section. The mean values and standard deviation of the eigenvalues can be directly evaluated from the scatter of the computed values. The continuous probability density function cannot be calculated directly from discrete response samples. Considering the Kernel density function [18] leads to an estimate of the probability density function from a discrete set of samples. The Kernel density estimation can be calculated as a weighted sum of Gaussian PDFs centered around these samples.

C. Perturbation Method

The real and imaginary parts of eigenvalues obtained by the Schur method at a fixed altitude can be expanded about the mean value of the uncertain structural parameters as

$$\gamma_i = \gamma_i(\hat{\theta}) + \mathbf{g}(\theta - \hat{\theta}) + \ldots \tag{9}$$

where $\mathbf{g} = [\partial\gamma_i/\partial\theta]$ is the first Jacobian, evaluated at the mean values of the structural parameters $\hat{\theta}$. The partial derivatives are evaluated at the mean structural parameters. Then $\hat{\gamma}_i = \gamma_i(\hat{\theta})$ and $\mathrm{Var}(\gamma_i) = \mathbf{g}(\hat{\theta})^T \mathrm{Cov}(\theta, \theta)\mathbf{g}(\hat{\theta})$. The PDFs of the real and imaginary parts of the aeroelastic eigenvalues can then be calculated using these expressions for the mean value and variance.

The first Jacobian matrix needs to be evaluated at the mean structural parameters to calculate the statistical moments. This is done in two stages. First, normal mode shapes and frequencies are calculated at perturbed values of the structural model parameters. Then, the Schur method is used to evaluate the aeroelastic eigenvalues at the perturbed parameter values. This is done using the Schur matrix already computed at the mean parameter values to drive the convergence of the quasi-Newton iterations for the perturbed normal mode shapes and frequencies (i.e., the residual function is evaluated for the perturbed normal mode shapes). For the first Jacobian, one nonlinear system needs to be solved for each structural parameter to obtain the Jacobian matrices for the real and imaginary parts of each aeroelastic eigenvalue.

D. Interval Analysis

An interval analysis defines a range for the uncertain structural parameters and then computes the possible range for the aeroelastic eigenvalues. The interval flutter problem is expressed as

$$\begin{cases} [\underline{\lambda}(\theta)_i, \bar{\lambda}(\theta)_i] = [\min(Re(\lambda_i)), \max(Re(\lambda_i))] \\ S(\lambda_i)\mathbf{p}_s - \lambda_i\mathbf{p}_s = 0, \\ \underline{\theta} \le \theta \le \bar{\theta} \end{cases} \tag{10}$$

The index i indicates the critical mode, and the under and over bars indicate the lower and upper bounds of the variable. A range for each of the variable structural parameters is chosen, and then an optimization problem must be solved to find the resulting range on the critical eigenvalue. In the current work a minimization function in Matlab (*fmincon*) that solves a constrained nonlinear multivariate problem is used. This method requires the parameter constraints (i.e., intervals on Θ) and a scalar objective function (denoted $\mathcal{C}$, which here is defined as the minimum or maximum real part of the critical eigenvalue). The computations are performed by a sequential quadratic programming (SQP) method [19–21].

First-order optimality is based on the Karush–Kuhn–Tucker (KKT) conditions. These conditions not only require the gradient of the objective function to be zero at a minimum but also consider the problem constraints. The KKT conditions are formulated via an approximate function of the Lagrangian, given by

$$\mathcal{L}(\theta, \varphi) = \mathcal{C} + \Sigma\varphi_j b_j(\theta) \tag{13}$$

where $b_j(\theta)$ represents the inequality and equality constraints shown in Eq. (10) and φ_j is the Langrange multiplier vector which has dimension equal to the number of constraints. At each major iteration, an approximation is made to the Hessian of the Lagrangian function using a quasi-Newton updating method. This is then used to generate a quadratic programming subproblem whose solution is used to form a search direction. The Hessian is updated at each major iteration of the SQP algorithm, using the Broyden, Fletcher, Goldfarb, and Shanno update method. The major computational cost is incurred in calculating the Jacobian of the eigenvalue with respect to the variable structural parameters Θ, which entails a Schur eigenvalue calculation for each uncertain structural parameter.

IV. Results

A. Goland Wing

The Goland wing, shown in Fig. 1, has a chord of 6 feet and a span of 20 feet. It is a rectangular cantilevered wing with a 4%-thick parabolic section. The structural model follows the description given in [22]. The CFD grid is block structured and uses an O–O topology. This allows points to be focused in the tip region, which is most critical for the aerodynamic contribution to the aeroelastic response. The fine grid has 250,000 points, and a coarse level was extracted from this grid with 40,000 points (which is used unless otherwise stated). Views of the fine grid are shown in Fig. 1. Four mode shapes were retained for the aeroelastic simulation. The Schur eigenvalue formulation was evaluated for the Goland wing test case in [11].

The main structural components of the wing are shown in Fig. 2. It is composed of upper and lower skins, 3 spars with caps, 11 ribs with caps, and 33 posts. There are two versions of the wing that are considered, namely with and without a tip store. The wing without a tip store is referred to as *clean*. The tip store is added to the clean wing by including a point mass at some streamwise location at the wing tip. The baseline tip-mass configuration has the mass located 0.25 ft from the leading edge. In both cases the parameters which define the geometry of the structural model are the thicknesses of the skins, the areas of the spar and rib caps, the thicknesses of the spars and ribs, and the areas of the posts. The mean values of these parameters follow those given in [6]. It should be noted that the density of the structural elements was taken to be negligible and the inertial properties are modeled as lumped mass elements shown in Fig. 2a.

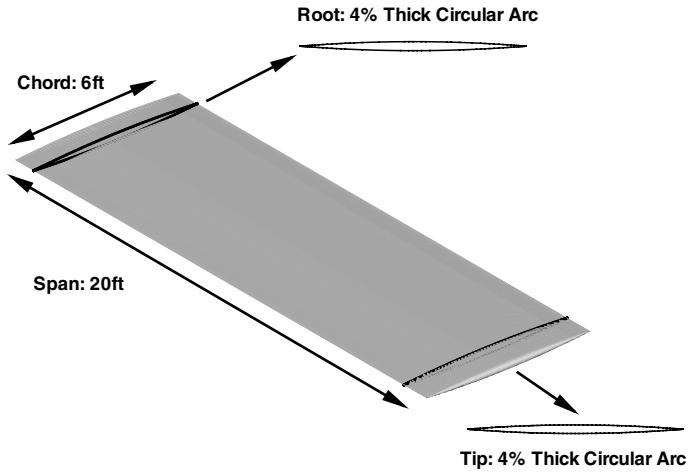

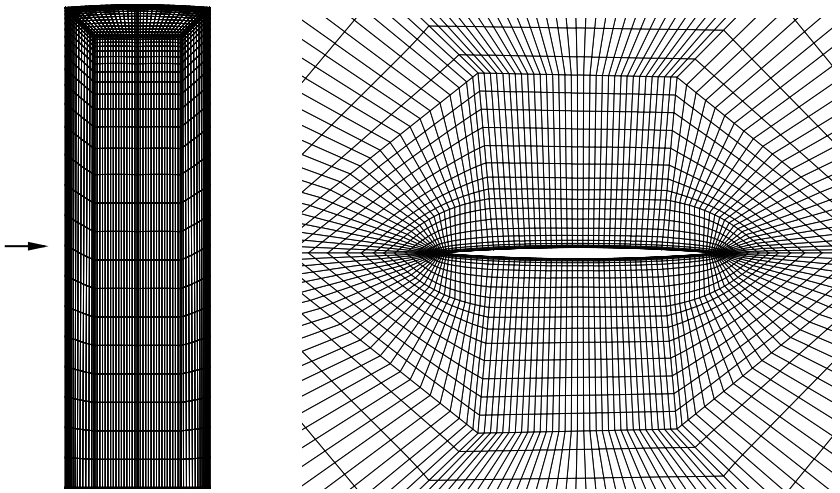

Fig. 1 Views of geometry and CFD grids for the Goland wing [11].

The sensitivity of the flutter speed for the clean wing to each of the structural parameters was previously calculated using a linear method [10]. This was done to indicate which structural parameters should be considered for the nonlinear analysis. The sensitivity of the aerodynamic damping at Mach 0.5 and sea level with respect to each parameter shows that there are seven parameters that are key to determining the flutter speed, namely the thicknesses of the leading and trailing-edge spars; the thicknesses of the upper and lower skins; and the areas of the leading-edge, trailing-edge, and center-spar caps.

B. Clean Wing Results

The clean wing flutter response was calculated at the mean structural parameters. This was done at Mach 0.5 for matched conditions. At Mach 0.5, an interaction between the wing first bending and torsion modes gives flutter between ground level and 10,000 ft. Although no transonic effects are present at this Mach number, the Euler-based Schur method was used to allow the feasibility (from a computational cost viewpoint) of the evaluation of the sensitivity of the flutter speed to structural parameters to be made.

The seven identified structural parameters were randomized by taking a coefficient of variation of 0.05 about the mean value, and a set of 1000 normal modes was generated. The series approximation was calculated at the mean parameter values, at a cost of 64 linear solves, and this matrix was then used to drive convergence of the quasi-Newton method for the random parameter combinations. The four aeroelastic eigenvalues were then computed for the 1000

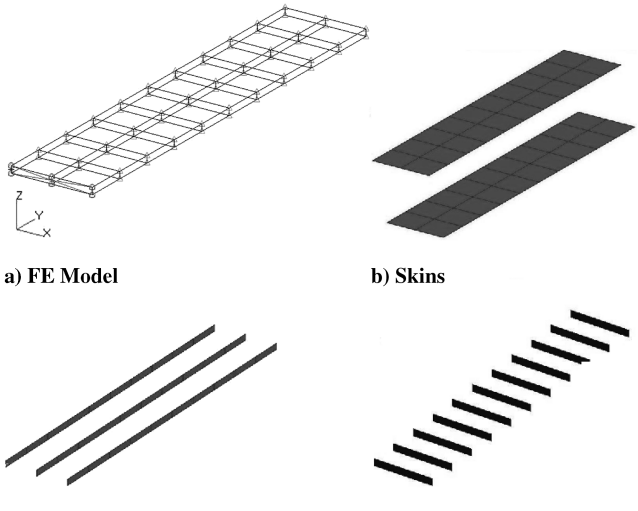

Fig. 2 Views of the main structural model components for the clean Goland wing.

Table 1 Converged structural parameter values for the maximum real part at different altitudes, scaled onto an interval $[-1, 1]$, for the Goland wing clean case at $M = 0.5$, $\alpha = 0°$

Parameter	Upper skin	Lower skin	LE spar	TE spar	LE spar cap	Center spar cap	TE spar cap
10,000 ft	−1.0	−1.0	−1.0	−1.0	1.0	1.0	1.0
9000 ft	−1.0	−1.0	−1.0	−1.0	1.0	1.0	1.0
2000 ft	−1.0	−1.0	−1.0	−1.0	1.0	1.0	1.0

samples. In each case the eigenvalues converged in 3–4 quasi-Newton steps, meaning that the computational cost at each altitude was 3–4 linear solves.

The linear perturbation method requires the calculation of the Jacobian of the aeroelastic eigenvalue with respect to each of the seven uncertain structural parameters at each altitude of interest, requiring 3–4 linear solves per parameter per altitude.

Finally, for the interval method the first step is to calculate the mean parameter aeroelastic eigenvalues. The eigenvalues that are close to becoming undamped and the range of critical altitude for these eigenvalues are selected. The interval analysis optimization is then run at these altitudes and for these eigenvalues. The Schur matrix is reevaluated at the mean value for each altitude chosen to drive rapid convergence for each function evaluation during the optimization. It was found that in the worst case around 12 optimization steps were required to achieve convergence to the maximum or minimum eigenvalue real part, needing 96 eigenvalue calculations. In total this took around 4 h of CPU time on a 3 GHz personal computer in the worst case to define both ends of the range.

For the maximum possible value for the real part of the eigenvalue the structural parameters converge to one or the other end of the parameter interval, as indicated in Table 1 where the uncertain parameters have been scaled onto the interval $[-1, 1]$. The skin and spar element thicknesses converge to the minimum allowed value when determining the maximum real part of the critical eigenvalue. The spar stiffness reduces with the cube of the thickness, and hence this parameter has a large influence in weakening the structure. The wing skins (which are represented by shell elements) and the spar elements have a larger influence on the torsional modes than the bending modes. A reduction of stiffness in these elements decreases the torsional structural frequencies. The spar cap areas are maximized by the optimization, which increases the stiffness of these elements. This raises the frequencies of the bending modes. The net effect is to bring the frequencies of the first bending and torsion

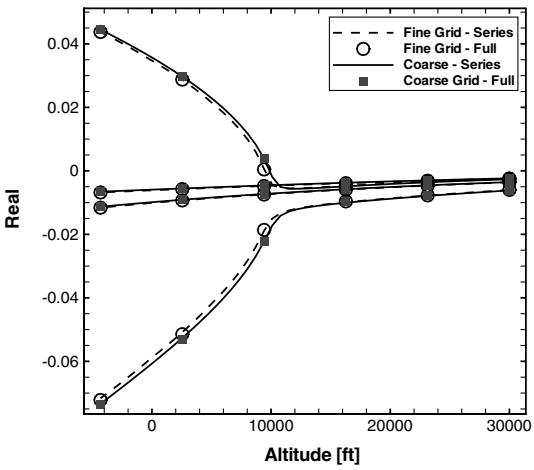

a) Mean Eigenvalues - Real Part

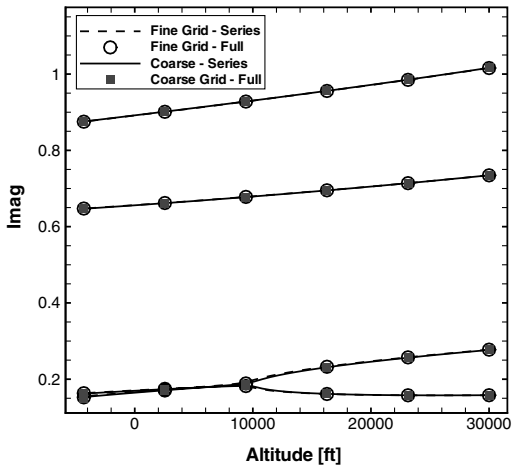

b) Mean Eigenvalues - Imaginary Part

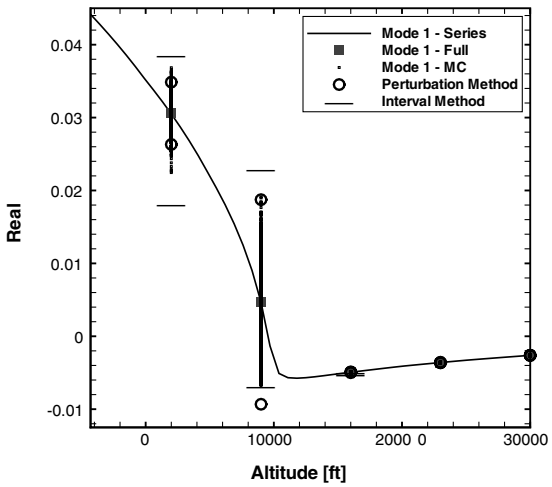

c) Variability on Mode 1 Eigenvalue Real Part

Fig. 3 Goland wing clean configuration mode tracking for $M = 0.5$, $\alpha = 0°$. MC refers to Monte Carlo, and the circles are the 2σ values from the perturbation PDF.

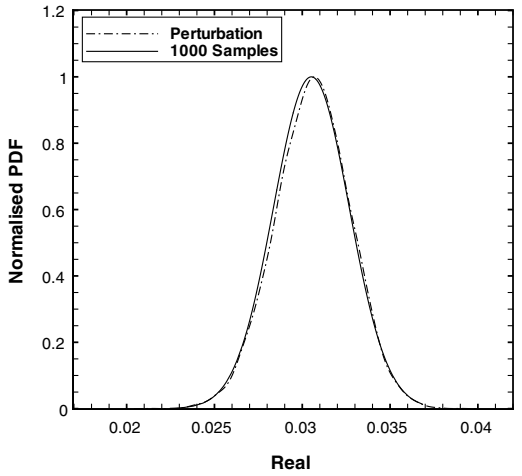

a) MC and Perturbation Method PDF

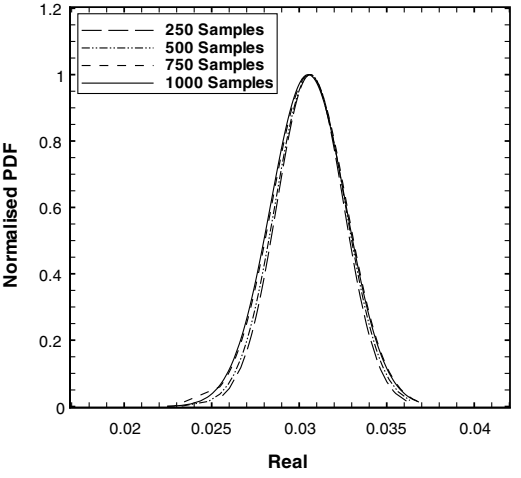

b) PDF Convergence for MC Analysis

Fig. 4 Normalized probability density functions: Goland wing clean case at $M = 0.5$, $\alpha = 0°$, 2000 ft.

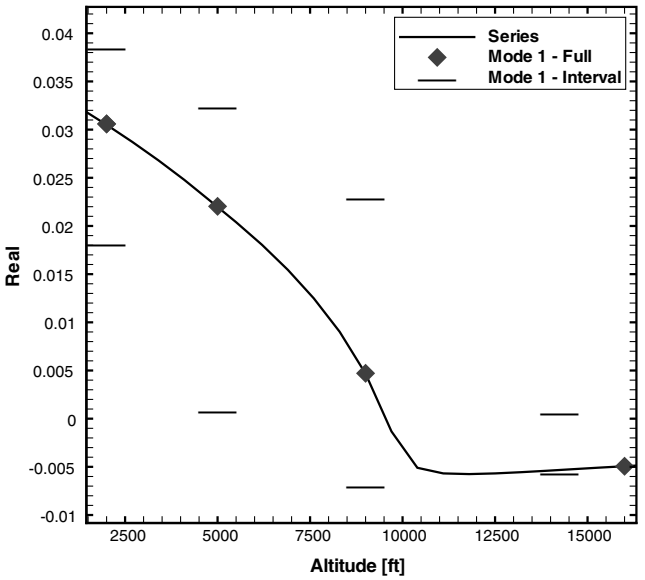

Fig. 5 Range of flutter altitude from interval analysis for Goland wing clean case at $M = 0.5$, $\alpha = 0°$.

modes closer together, reducing the stability (increasing the aeroelastic eigenvalue real part) of these interacting modes. For the minimum possible value (which is of less interest), some parameter values converge to internal values.

The mode tracking, together with the influence of structural variability, is shown in Fig. 3. In this figure the lines indicate the eigenvalues predicted using the series approximation to the residual of Eq. (6) whereas the points are from a full evaluation at that altitude. The two sets of results are in perfect agreement for this case. Results are shown on the coarse and fine grids, which are in close agreement. In Figs. 3a and 3b the mean parameter mode tracking is shown. The interaction of the modes, which, with the wind off, are the first wing bending and torsion modes, is clear in Fig. 3b with the convergence of these frequencies below 10,000 ft. The bending mode becomes undamped, as shown in Fig. 3a. The influence of structural variability is shown at three altitudes in Fig. 3c. This figure includes the Monte Carlo simulation results (with each sample indicated by one point on the graph), the perturbation results (with the 2σ results indicated by circles), and the interval maximum and minimum indicated by the lines. The first observation is that the scatter of the results on the real part of the eigenvalue is very small before the modes start to interact strongly. After this interaction starts the spread of results grows dramatically. The interval results capture the Monte Carlo samples. The PDFs at 2000 ft from the Monte Carlo and perturbation methods are shown in Fig. 4. There are minor differences in the tails. In addition, the convergence of the PDF with an increasing number of samples is shown, demonstrating good convergence even with 250 samples.

Interval calculations at a number of altitudes allow lower and upper interval bounds to be traced as a function of altitude. These curves are shown in Fig. 5, which shows that the altitude range for flutter onset is from 14,000 to 5000 ft.

The costs of the different approaches are shown in Table 2. These costs are shown both in terms of the number of eigenvalue calculations and also the CPU time on a Pentium 3 GHz processor (i.e., a desktop computer). The linear perturbation method has a small cost but cannot capture skewness in the PDF if this is present. The interval method requires up to 4 h to define the worst-case interval. Finally, even the Monte Carlo simulation only requires 50 h for 1000 samples.

Given that the choice of variability in the structural parameters is likely to be based on the intuition of an analyst rather than on hard statistical data, the essential information in the results of these analyses is in the spread of the results rather than in the PDF. If this is accepted then the interval results have a good balance between capturing the spread (including any skewness) and the computational cost, and it will be used for the remaining cases in this paper.

C. Tip Store Results

The Goland wing with a tip store is an interesting case because there is a Mach number range above 0.92 that features a rapid reduction in stability and the appearance of limit cycle oscillations. An important contribution to this behavior comes from the development of a strong shock wave. The flutter boundary in terms of the critical altitude as a function of Mach number is shown in Fig. 6. The rapid loss of stability is indicated by the boundary heading vertically up on the figure at Mach 0.92. The critical mode switches around this Mach number from the first (mode 1) to the second (mode 3) bending, as annotated on the figure. The same structural

Table 2 Comparison of methods to calculate the eigenvalue real part variability for the critical mode at one altitude for the Goland wing clean case

Method	Number of eigenvalue evaluations	Wall clock time
Monte Carlo	1000	50 h
Perturbation	7	21 min
Interval	60–190	2.5–8 h
Single flutter point	1	3 min

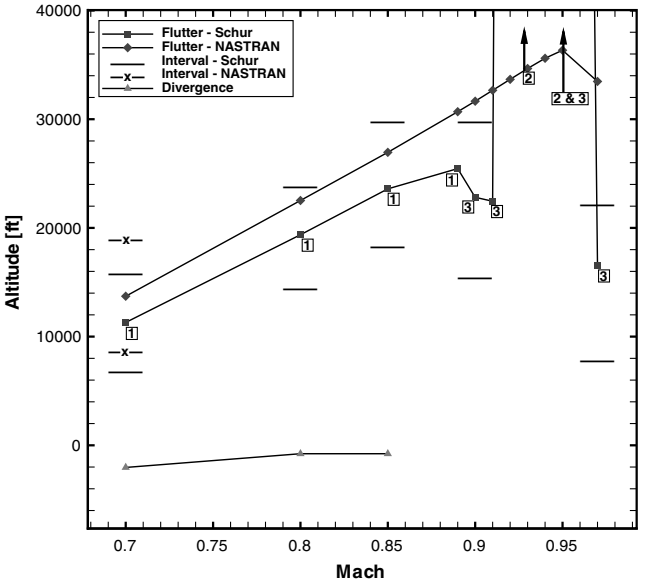

Fig. 6 Instability boundary: Goland wing store case. The numbers in squares indicate the unstable mode in the CFD-based results.

parameter variation is applied as for the clean wing. The intervals on the flutter altitude are included in Fig. 6. Also included on the figure is the mean parameter prediction from the linear analysis commercial code MSC NASTRAN, which uses the classical doublet-lattice method for the aerodynamics [23]. The main difference with the CFD-based results comes around values of Mach number of 0.92 where the shock is destabilizing, an effect not seen by the linear predictions. Also, the uncertain interval for the linear results is included at Mach 0.7 and is very similar in extent to the CFD-based interval at this Mach number. The modal interaction results at Mach 0.9 are shown in Fig. 7. Throughout the Mach number range the first mode is lightly damped, and the structural variability creates a significant variation on the flutter altitude, as illustrated in Fig. 7c. It is, however, interesting to note that the variation in the flutter altitude does not increase as the Mach number approaches the critical value (0.92) where the stability is rapidly lost due to aerodynamic effects.

D. Generic Fighter Model

Having demonstrated the approach on a model wing, a second case is computed to show feasibility on a realistically sized aircraft model. The intention here is to show that the method can scale to models of the size required for the analysis of aircraft. The generic fighter was built on data publically available for the F-16 aircraft, since this has been the subject of much interest from an aeroelastic viewpoint. The approach was to establish a test case which is recognizable as an aircraft, but the model does not replicate the actual behavior of the F-16. Available data for the wing geometry (dimensions and aerofoil section), together with published data from ground vibration tests (GVT) and wind tunnel data, was used.

The geometry is summarized in Fig. 8 and is an extension of that described in [11]. The basic shape of this model started from an artistic CAD model of the F-16. The model has several inaccuracies

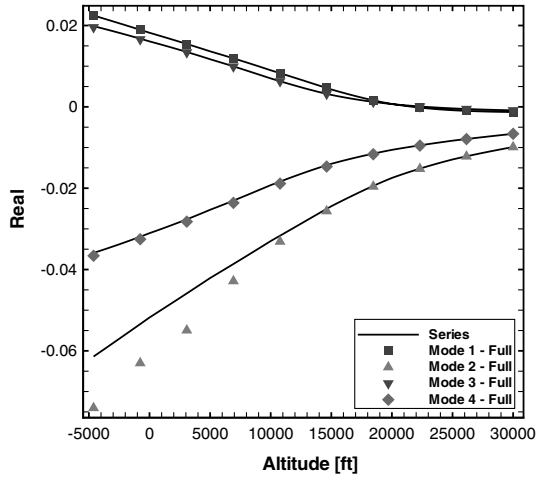

a) Mean Eigenvalues - Real Part

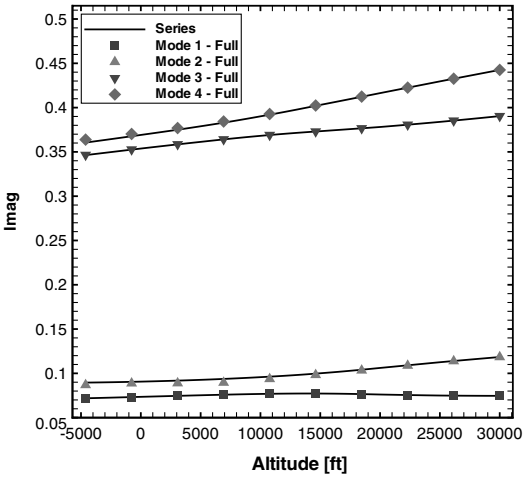

b) Mean Eigenvalues - Imaginary Part

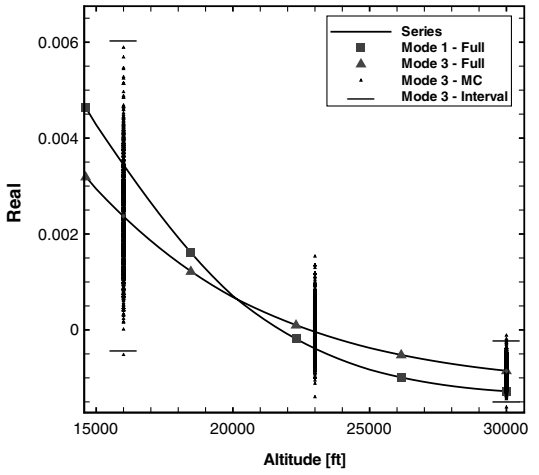

c) Variability on Mode 3 Eigenvalue - Real Part

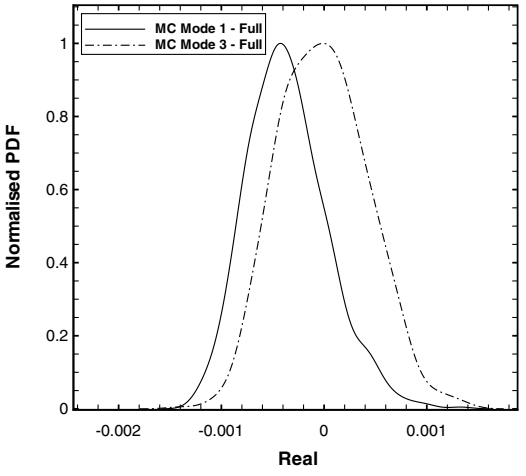

d) PDF of Modes 1 and 3 real parts

Fig. 7 Eigenvalue variation with altitude at $M = 0.9, \alpha = 0°$ for the Goland wing store case.

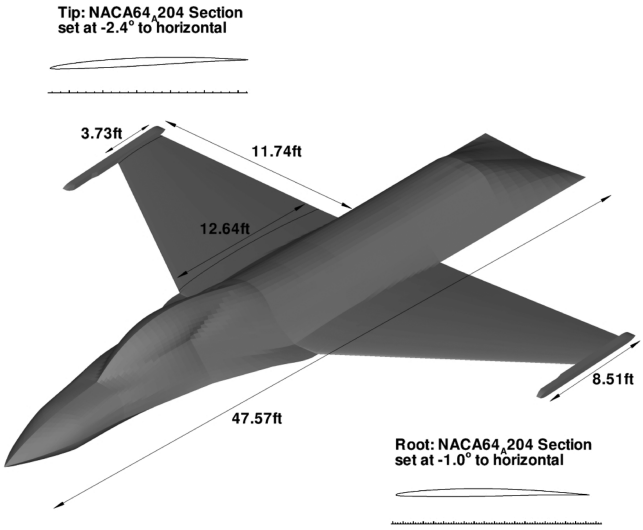

Fig. 8 Generic fighter geometry and surface CFD grid.

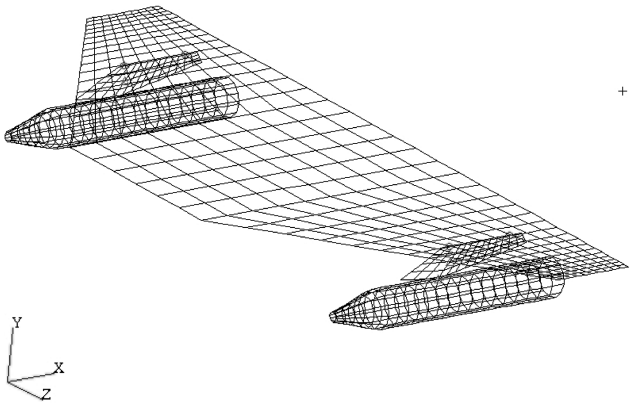

Fig. 10 Structural FE model for the generic fighter.

with respect to the fuselage geometry; however, it is thought that a reasonable first generic test case can be obtained without the exact fuselage and tail aerodynamics. In the first version of the model the tail plane has been removed. The aerofoil section consists of a NACA 64A204 profile, with a wing root angle of $-1°$ and a wing tip angle of $-2.4°$. The twist was chosen by comparing with published surface pressures for the F-16 [24] at a free stream Mach number of 0.85 at an angle of attack of 2.12°. The untwisted wing developed a strong shock wave. To mitigate this, the effective angle of attack was reduced by adding nose down twist at the wing tip. The upper and lower surfaces were then generated by sweeping the tip aerofoil up to the wing root. A few iterations were necessary to obtain the value of twist at the tip.

From the definition of the geometry, a H-type block structured grid was used around the wing and a C-type block topology was applied around the fuselage. A coarse grid was generated with 1.06 million points and 344 blocks for the full configuration. This was extracted from a fine grid with 8.5 million points for the full configuration. The calculations presented are on the coarse grid unless otherwise stated. The surface grid is shown in Fig. 8 and shows that the points are concentrated on the wing. Figure 9 shows the comparison with wind tunnel measurements of the surface pressures at two locations along the span. The untwisted wing solution is included for comparison. The solutions on the coarse and fine grids are in close agreement.

The finite element (FE) model of the wing was built in NASTRAN based on the model proposed by Cattarius [25] and is shown in Fig. 10. The structural model consists of four parts: fuselage, wing, pylon, and stores. The fuselage was modeled by using shell elements (QUAD4). The fuselage, pylon, and stores are considered to be effectively rigid. The mass properties of the pylon and stores are represented by lumped masses of values 11.032 and 70.406 slugs, respectively. The principal moments of inertia of the store are 652.6 lb ft^2 about its axis, aligned with the streamwise flow direction, and 23730 lb ft^2 about the other two axes. The triangular elements, shown in Fig. 10, indicate a lump mass element. The pylon is rigidly connected to the wing. The store is connected to the pylon by six spring elements (three translational and three rotational). The wing is also modeled using shell elements (QUAD4) and is divided into three regions: root, pylon, and tip. To match the natural frequencies of the FE model to those found in the GVT [26], the

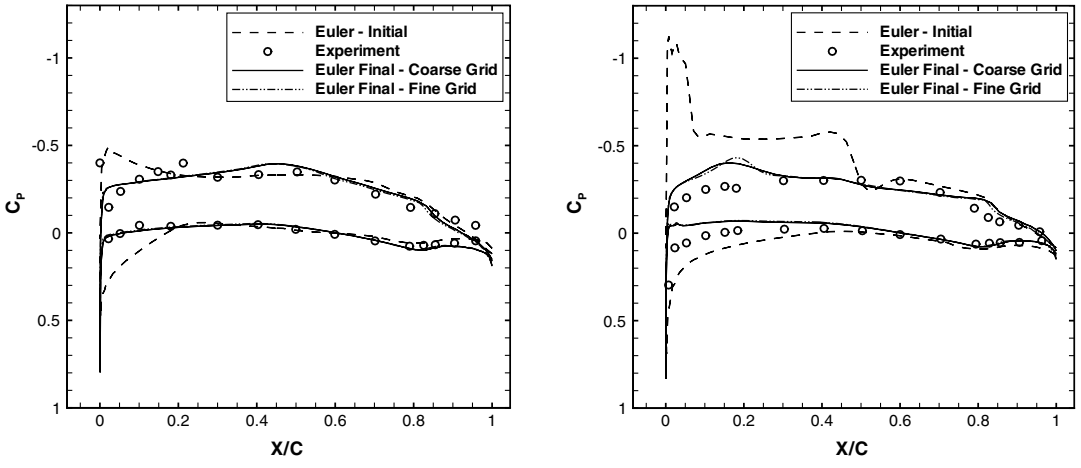

a) 59% Span **b) 85% Span**

Fig. 9 Surface pressure comparison for generic fighter: $M = 0.85, \alpha = 2.12°$. Initial: untwisted wing. Final: tip twist of $-2.4°$. The measurements are from [24].

Table 3 Wing shell element properties for generic fighter

Property	Wing (inner)	Wing (mid)	Wing (outer)
E [psi $\times 10^6$]	22.8	14.0	13.9
G [psi $\times 10^6$]	9.1	5.6	5.5
ρ [lb/in^3]	0.25	0.25	0.25
t [in]	2.95	1.18	1.18

Table 4 Symmetric mode frequencies for generic fighter

	Mode 1	Mode 2	Mode 3	Mode 4
Updated FE model	3.74 h_1	5.91 $\alpha + \theta$	8.12 γ	11.0 $h_2 + \alpha$
GVT [26]	4.07 h_1	5.35 $\alpha + \theta$	8.12 γ	12.25 h_2

[a]h_i is ith bending; α is pitch; θ is torsion; γ is yaw

Young's modulus and density of each region of the wing are considered as updating parameters [27,28]. Updated properties are given in Table 3. Table 4 shows the first four symmetric natural frequencies of the updated FE model and GVT data. Note that the GVT data was only available for the symmetric modes. Figure 11 shows the first eight mode shapes of the full model including both symmetric and antisymmetric modes. The mapping between the CFD and FEM grids was done using the transformation method described in [29]. The two wings are connected by a plate in the structural model, and this plate is used to drive the aerodynamic grid on the fuselage.

A linear sensitivity analysis for the flutter speed against the structural parameters was again carried out using NASTRAN [23]. This identified the most important structural parameters as being the rotational spring coefficient for the store attachment; the Young's modulus of the wing root and pylon sections; and the densities for the wing root, tip, and pylon regions. An interval was defined for each of these parameters as $\pm 15\%$ for the rotational spring coefficient and $\pm 10\%$ for the other parameters.

The Schur flutter analysis for the mean and varying structural parameters is shown in Fig. 12. In Figs. 12a and 12b the real and imaginary parts at the mean structural parameters are shown for all modes. The antisymmetric second and third modes interact, with the third mode going undamped at about 6562 ft. The intervals for mode 3 at three altitudes are shown in Fig. 12c. Also added at the middle altitude are eight randomly computed samples, which all lie within the computed interval. Similar behavior to the Goland wing is observed; i.e., the interval grows significantly after the modal interaction becomes strong. Before the interaction starts, the eigenvalue real parts are not significantly affected by variation in the structural stiffness (and mass). Close to flutter the structural stiffness terms become important to the damping through aerodynamic coupling. And so, the interval on the real part of the eigenvalue increases greatly as flutter is approached and beyond because of stiffness variability. Again the mean parameter matrices were used to drive convergence of the Schur calculations during the optimization. This was done on 44 processors of a PC cluster and took around 7 h. The structural variation chosen was high in this case and the mean matrices were not sufficient to drive convergence for some extreme parameter values. If Newton convergence is not observed then the iterations are stopped, the Schur matrices regenerated to provide a better Jacobian to drive convergence, and the iterations restarted.

An assessment of the variability over high subsonic freestream Mach numbers is shown in Fig. 12d. Figure 12a shows mode 3 to be

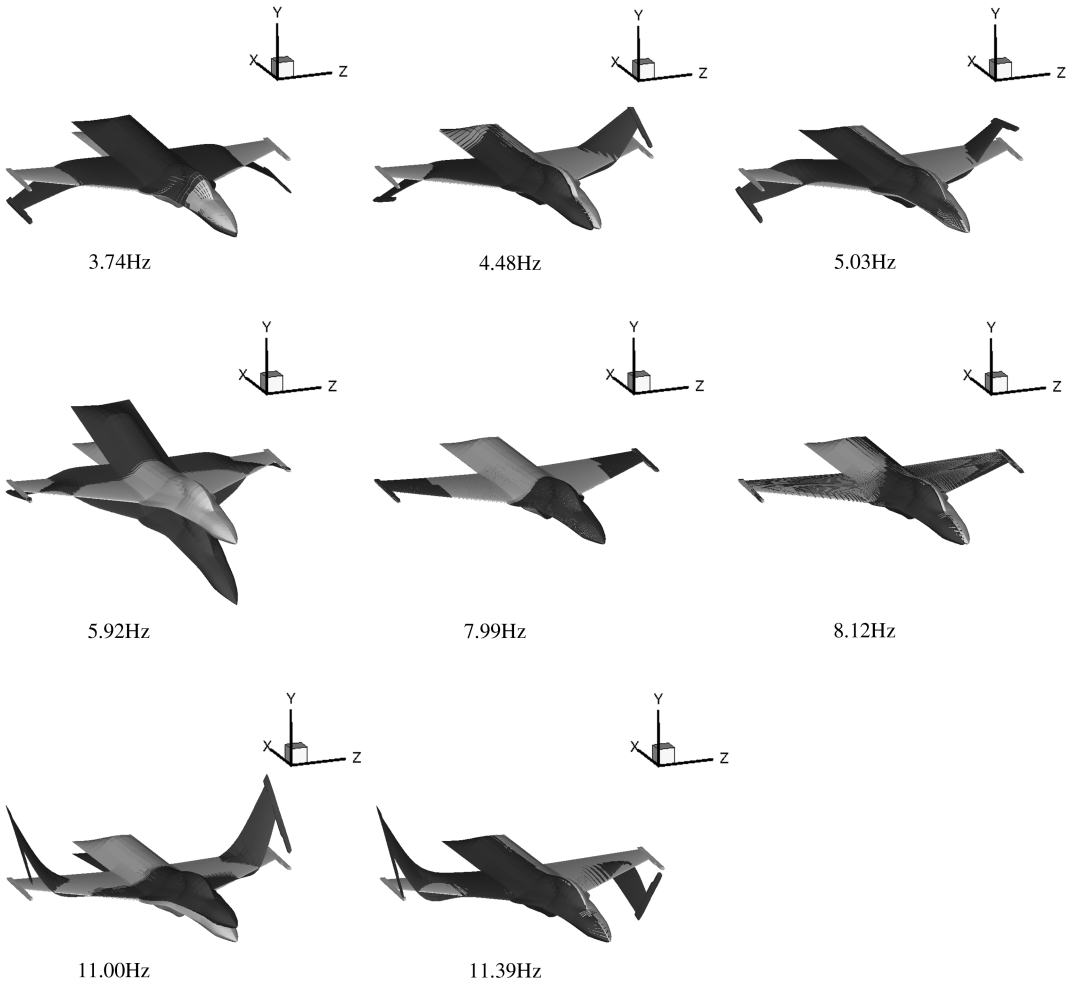

Fig. 11 Mapped structural normal modes for the generic fighter.

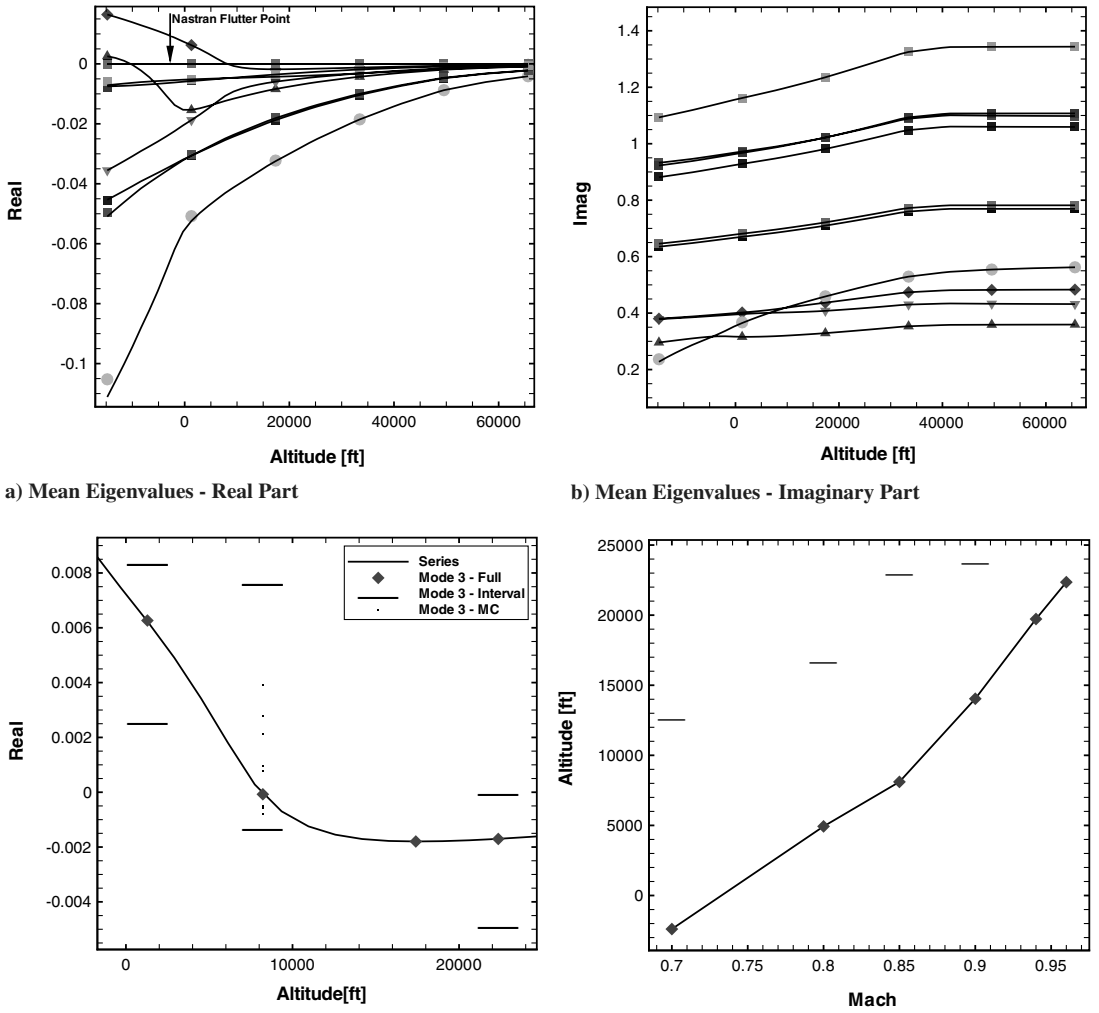

a) Mean Eigenvalues - Real Part

b) Mean Eigenvalues - Imaginary Part

c) Variability on Mode 3 Eigenvalue - Real Part

d) Flutter boundary uncertainty

Fig. 12 Eigenvalue variation with altitude at $M = 0.85, \alpha = 0°$ for the generic fighter case. Lines from the series approximation and points from the full nonlinear solution.

lightly damped. Small changes to this mode can lead to large variations in the flutter altitude. Linear calculations using NASTRAN showed that mode 1 is the mode to become undamped, which for most of the envelope is not near the instability boundary and therefore can withstand structural variations for larger parts of the flight envelope. The flutter boundary shown in Fig. 12d also allows the flutter onset Mach number at a fixed altitude to be estimated. The flutter altitude at $M = 0.8$ for the mean structural parameters is 4921 ft and at $M = 0.91$ is 16,404 ft. From the interval analysis shown in Fig. 12d, flutter at $M = 0.8$ can develop at 16,404 ft within the range of structural variation assumed.

V. Conclusions

The feasibility of using three methods to propagate structural model variability to aeroelastic stability prediction has been investigated. The methods considered were Monte Carlo simulation, perturbation analysis, and interval analysis. The feasibility in terms of computational cost was demonstrated, when using CFD, by exploiting an eigenvalue-based method, which can be configured for the purpose of computing stability for many similar structural models. A rapid increase in the sensitivity of the real part of the critical eigenvalue to the structural variability was observed after the modal interaction starts. Two test cases were considered, the first based on the Goland wing and the second on a generic fighter. The most important structural parameters for flutter were determined through a linear sensitivity analysis, and in this way O(10) parameters were chosen for the variability analysis. For the Goland wing, 1000 structural samples were computed in two days on a desktop PC and the interval results in around 3 h.

An interesting question is how to use these methods for applications. The generation of probability distributions by Monte Carlo analysis and perturbation analysis is attractive for certification applications, but this attraction may be deceptive. These distributions must be interpreted in the light of the definition of the structural variation distributions. These are likely to be based on the best guess of the analyst since hard data is unlikely to be available. In these circumstances the important information is in the spread of the eigenvalue real parts. The interval method captures this spread, and also skewness about the mean, in a reasonable computational cost. This method is therefore favored based on this consideration.

Current work is focusing on extending the approach demonstrated in this paper to include more influences on the stability predictions and to understand the routes by which structural parameter uncertainty can influence aeroelastic stability. The current work has not included the influence of altitude on the static equilibrium of which the stability is computed. This effect can be introduced by updating the static equilibrium at each altitude and updating the matrices used in the eigenvalue problem at this state. Structural variability can influence aeroelastic stability through changing the normal mode frequencies, mode shapes, and the static equilibrium. The question of which of these sources is significant for any given

problem is interesting because the answer provides options for simplifying the variability calculation as well as providing physical insight. These investigations are currently being carried out.

Acknowledgements

This work is funded by the European Union for the Marie Curie Excellence Team Enabling Certification by Analysis (ECERTA) under contract MEXT-CT-2006 042383.

References

[1] Pettit, C., "Uncertainty Quantification in Aeroelasticity: Recent Results and Research Challenges," *Journal of Aircraft*, Vol. 41, No. 5, 2004, pp. 1217–1229. doi:10.2514/1.3961

[2] Walters, R., and Huyse, L., "Uncertainty Analysis for Fluid Mechanics with Applications," NASA CR 2002-211449, Feb. 2002.

[3] Pitt, D., Haudrich, P., and Thomas, M., "Probabilistic Aeroelastic Analysis and its Implications on Flutter Margin Requirements," AIAA Paper 2008-2198, April 2008.

[4] Ghanem, R., and Spanos, P., "Stochastic Finite Elements: a Spectral Approach," Dover, New York, 2003.

[5] Majumder, L., and Rao, S., "Interval-based optimization of aircraft wings under landing loads," *Computers and Structures*, Vol. 87, No. 3–4, 2009, pp. 225–235. doi:10.1016/j.compstruc.2008.10.005

[6] Kurdi, M., Lindsley, N., and Beran, P., "Uncertainty Quantification of the Goland Wing's Flutter Boundary," AIAA Paper 2007-6309, Aug. 2007.

[7] Willcox, K., and Peraire, J., "Application of Reduced-Order Aerodynamic Modeling to the Analysis of Structural Uncertainty in Bladed Disks," American Society of Mechanical Engineers Paper GT-30680, June 2002.

[8] Verhoosel, C., Scholcz, T., Hulshoff, S., and Gutiérrez, M., "Uncertainty and Reliability Analysis of Fluid-Structure Stability Boundaries," *AIAA Journal*, Vol. 47, No. 1, 2009, pp. 91–102. doi:10.2514/1.35770

[9] Rao, S., and Majumder, L., "Optimization of Aircraft Wings for Gust Loads: Interval Analysis-Based Approach," *AIAA Journal*, Vol. 46, No. 3, 2008, pp. 723–732. doi:10.2514/1.33152

[10] Khodaparast, H. H., Mottershead, J. E., and Badcock, K. J., "Propagation of Structural Uncertainty to Linear Aeroelastic Stability," *Computers and Structures* (to be published).

[11] Badcock, K. J., and Woodgate, M. A., "Prediction of Bifurcation Onset of Large Order Aeroelastic Models," AIAA Paper 2008-1820, May 2008.

[12] Osher, S., and Chakravarthy, S., "Upwind Schemes and Boundary Conditions with Applications to Euler Equations in General Geometries," *Journal of Computational Physics*, Vol. 50, No. 3, 1983, pp. 447–481. doi:10.1016/0021-9991(83)90106-7

[13] Van Leer, B., "Towards the Ultimate Conservative Difference Scheme II: Monotonicity and Conservation Combined in a Second Order Scheme," *Journal of Computational Physics*, Vol. 14, No. 4, 1974, pp. 361–374. doi:10.1016/0021-9991(74)90019-9

[14] Badcock, K. J., Richards, B. E., and Woodgate, M. A., "Elements of Computational Fluid Dynamics on Block Structured Grids Using Implicit Solvers," *Progress in Aerospace Sciences*, Vol. 36, Nos. 5–6, 2000, pp. 351–392. doi:10.1016/S0376-0421(00)00005-1

[15] Badcock, K. J., Woodgate, M. A., and Richards, B. E., "The Application of Sparse Matrix Techniques for the CFD based Aeroelastic Bifurcation Analysis of a Symmetric Aerofoil," *AIAA Journal*, Vol. 42, No. 5, 2004, pp. 883–892. doi:10.2514/1.9584

[16] Badcock, K. J., Woodgate, M. A., and Richards, B. E., "Direct Aeroelastic Bifurcation Analysis of a Symmetric Wing Based on the Euler Equations," *Journal of Aircraft*, Vol. 42, No. 3, 2005, pp. 731–737. doi:10.2514/1.5323

[17] Bekas, K., and Saad, Y., "Computation of Smallest Eigenvalues Using Spectral Schur Complements," *Journal of Scientific Computing*, Vol. 27, No. 2, 2005, pp. 458–481. doi:10.1137/040603528

[18] Bowman, A. W., and Azzalini, A., *Applied Smoothing Techniques for Data Analysis*, Oxford Univ. Press, Oxford, U.K., 1997.

[19] Gill, P. E., Murray, W., and Wright, M. H., *Practical Optimization*, Academic Press, London, 1981.

[20] Han, S. P., "A Globally Convergent Method for Nonlinear Programming," *Journal of Optimization Theory and Applications*, Vol. 22, No. 3, 1977, p. 297. doi:10.1007/BF00932858

[21] Powell, M. D., "A Fast Algorithm for Nonlinearly Constrained Optimization Calculations," *Lecture Notes in Mathematics*, Vol. 630, 1978, pp. 144–157. doi:10.1007/BFb0067703

[22] Beran, P. S., Knot, N. S., Eastep, F. E., Synder, R. D., and Zweber, J. V., "Numerical Analysis of Store-Induced Limit Cycle Oscillarion," *Journal of Aircraft*, Vol. 41, No. 6, 2004, pp. 1315–1326. doi:10.2514/1.404

[23] Giesling, J. P., Kalman, T. P., and Rodden, W. P., "Subsonic Steady and Oscillatory Aerodynamics for Multiple Interfering Wings and Bodies," *Journal of Aircraft*, Vol. 9, No. 10, 1972, pp. 693–702. doi:10.2514/3.59066

[24] Denegri, C., and Dubben, J., "F-16 Limit Cycle Oscillation Analysis Using Transonic Small-disturbance Theory," AIAA Paper 2005-2296, April 2005.

[25] Cattarius, J., "Numerical Wing/Store Interaction Analysis of a Parametric F-16 Wing," Ph.D. dissertation, Virginia Polytechnic Institute and State University, Blacksburg, VA, 1999.

[26] Cazier, F. W., Jr., and Keloe, M. W., "Ground Vibration Test on an F-16 Airplane with Modified Decoupler Pylons," NASA-TM-87634, 1986.

[27] Mottershead, J. E., and Friswell, M. I., "Model Updating in Structural Dynamics: a Survey," *Journal of Sound and Vibration*, Vol. 167, No. 2, 1993, pp. 347–375. doi:10.1006/jsvi.1993.1340

[28] Khodaparast, H. H., Mottershead, J. E., and Friswell, M. I., "Perturbation Methods for the Estimation of Parameter Variability in Stochastic Model Updating," *Mechanical Systems and Signal Processing*, Vol. 22, No. 8, 2008, pp. 1751–1773. doi:10.1016/j.ymssp.2008.03.001

[29] Woodgate, M. A., Badcock, K. J., Rampurawala, A. M., Richards, B. E., Nardini, D., and Henshaw, M. J., "Aeroelastic Calculations for the Hawk Aircraft Using the Euler Equations," *Journal of Aircraft*, Vol. 42, No. 4, 2005, pp. 1005–1012. doi:10.2514/1.5608